Separation and Purification Technology 308 (2023) 122915

Contents lists available at ScienceDirect

Separation and Purification Technology

journal homepage: www.elsevier.com/locate/seppur

Nanofiltration with polyamide thin film composite membrane with ZIF-93/SWCNT intermediate layers on polyimide support

Victor Berned-Samatán [a,b], Marten Piantek [c], Joaquín Coronas [a,b], Carlos Téllez [a,b,*]

[a] Instituto de Nanociencia y Materiales de Aragón (INMA), CSIC-Universidad de Zaragoza, Zaragoza 50018, Spain
[b] Chemical and Environmental Engineering Department, Universidad de Zaragoza, Zaragoza 50018, Spain
[c] Laboratorio de Microscopias Avanzadas, Instituto de Nanociencia y Materiales de Aragón (INMA), CSIC-Universidad de Zaragoza, Zaragoza 50018, Spain

ARTICLE INFO

Keywords:
Nanofiltration
Metal-organic framework layer
Carbon nanotubes layer
Thin film composite membrane
Polyamide

ABSTRACT

Among current separation processes, nanofiltration (NF), besides its easy scalability, exhibits low energy consumption, environmental impact and footprint, being widely used for water treatment and solvent recovery. The development of membranes for NF involves perfecting the skin selective layer, the sublayers and the support. In this work, a multilayer structure membrane is presented where a selective layer of polyamide (PA, thickness 40–60 nm) was interfacially polymerized on a sub-layer of MOF ZIF-93 (thickness ~ 50 nm) grown on another sub-layer of single-walled carbon nanotubes (SWCNT, thickness ~ 400 nm) vacuum filtrated on an asymmetric polyimide P84® support (thickness ~ 200 μm). The membrane with structure PA/ZIF-93/SWCNT/P84 showed excellent results in water NF and methanol organic solvent NF of different dyes (with the highest values of water and methanol permeances of up to 57.6 and 84.5 $L{\cdot}m^{-2}{\cdot}h^{-1}{\cdot}bar^{-1}$, respectively, with rejections usually greater than 99%). By means of a wide range of characterization techniques (contact angle, AFM, XRD, ATR-FTIR and FIB-SEM) the role of every component in the membrane was elucidated. In fact, the presence of the sublayer of ZIF-93 increased the roughness and hydrophilicity as well as decreased the thickness of the PA layer. These effects are related to the fact that the sublayers subordinate the interfacial polymerization as well as influence the properties of the PA film and therefore its NF performance, even showing chlorine resistance as well as ten-day cross-flow NF stability.

1. Introduction

Membrane technology is a process that, with respect to the classic separation processes (e.g. distillation, absorption, liquid–liquid extraction), can be considered more energy efficient, smaller in footprint and more environment friendly, being also a continuous modular process, which can operate easily and is easy to scale [1]. Nanofiltration is a pressure-driven membrane process that present higher fluxes with respect to reverse osmosis membranes, low rejection of monovalent salts, high rejection of divalent salts, molecular weight cut-off (smallest molecular size of the solute in which the membrane has a rejection equal to or greater than 90%) in the 150–2000 Da range, pore size less than 2 nm and working pressures in the 5–35 bar range [2–5].

Nanofiltration has been applied in the treatment of water and wastewater as well as in desalination and in industries related to the recovery or obtaining of biotechnology products, food additives, flavours or pharmaceutical products, among other fine chemicals [6,7]. When the solvent is an organic compound, organic solvent nanofiltration (OSN) has been defined, which has a great application in the industries mentioned above for the recovery of the solvents used in organic synthesis or in washing processes [4].

Nanofiltration membranes can be classified in two main types: the so-called integrally skinned asymmetric (ISA) membranes prepared by phase inversion and the called thin film composite (TFC) membranes where a selective thin layer is typically placed on top of an asymmetric porous support. Compared to ISA membranes, TFC membranes have the advantages of lower cost on the polymer of the selective layer, allow optimization of the composition and structure of the selective layer and the support independently, in order to obtain the best separation properties under stable operating conditions, and have fewer mechanical limitations [8]. TFC membranes can be prepared by interfacial polymerization (IP) [9], probably the most used method since it allows to control the formation of ultra-thin layers. In the IP, the selective layer is usually a polyamide (PA) thin film formed by a reaction at the interface

* Corresponding author at: Instituto de Nanociencia y Materiales de Aragón (INMA), CSIC-Universidad de Zaragoza, Zaragoza 50018, Spain.
E-mail address: ctellez@unizar.es (C. Téllez).

https://doi.org/10.1016/j.seppur.2022.122915
Received 18 October 2022; Received in revised form 30 November 2022; Accepted 11 December 2022
Available online 14 December 2022

between two immiscible liquids (water-organic). Usually, the support is first impregnated with a diamine (m-phenylenediamine (MPD) and piperazine (PIP) being the most used) in aqueous phase and then impregnated with an acyl halide (most used trimesoyl chloride, TMC) in an organic solvent. There are different approaches to improve the performance (permeance/rejection), the antifouling properties and the chlorine resistant of TFC membranes prepared by IP [5,9,10]. Alternative strategies have also been carried out such as vapour phase interfacial polymerization or inverse IP (iIP) where the order of impregnation of the phases during IP is changed [5,9,11].

It is evident that the sublayer where the PA is formed affects, on the one hand, the layer formation process during the IP, changing the properties of the PA layer such as thickness, surface roughness, hydrophilicity or crosslinking. On the other hand, the porous structure and the hydrophilicity/hydrophobicity of the sublayer can play an important role in the nanofiltration performance [10,12]. Therefore, a method to improve TFC membranes consists of the use of a nanostructured material as an interlayer between the PA and the support: PA/MOF on polyimide (PI) [13,14] or poly(ether sulfone) (PES) supports [15], PA/2D MOF on PES support [16], PA/COF on polyacrylonitrile (PAN) [17] or PI [18] supports and PA/based CNTs on PES support [19–23].

In our earlier study [24], self-standing single walled carbon nanotubes buckypapers (SWCNT-bp) were used as support due their chemical stability and mechanical strength. This support was used to grow a PA layer by iIP or a bilayer membrane in which the PA layer was formed via iIP on top of a MOF layer (Fig. 1A) obtaining in both cases outstanding results in NF and OSN of dyes and salts. The improved separation performance was related to a more accurate control of the polyamide layer synthesis during the IP and, in consequence, to changes in the properties of the PA, especially roughness and hydrophilicity. The MOF that gave the best results was ZIF-93, which belongs to the zeolitic imidazole framework (ZIF) family of MOFs with zeolitic topologies. The hydrophilic ZIF-93 (Zn(4-methyl-5-imidazolatecarboxaldehyde)$_2$) has a framework with RHO zeolitic topology (Fig. 1C) and also has the interesting properties of MOFs: high specific surface area, high pore volume, control in the synthesis of particle size, adsorption properties and organic–inorganic character, which makes them simultaneously compatible with both polymers and inorganic materials.

Herein, we report a four layer complex membrane structure (PA/ZIF-93/SWCNT/P84, Fig. 1B) which improves our previous work (PA/ZIF-93/SWCNT-bp, Fig. 1A) since the amount of SWCNT is notably reduced by 99.5% with the use of the polymeric support (polyimide P84®) increasing the mechanical robustness and processability of the final membrane without lessen its separation performance. As an example of the removal of pollutants from water and OSN, nanofiltration of water and methanol with dyes in the range of 265–1017 Da of molecular weight will be carried out. In addition, nanofiltration of divalent and monovalent salts and the resistance to chlorine will be verified. Finally, with the characterization of the samples, the function of the intermediate layers will be established. The main role of the SWCNT layer is to provide an effect of gutter layer for the ZIF-93 synthesis and the role of ZIF-93 layer is to control the IP changing the properties of the polyamide layer.

2. Experimental

2.1. Preparation of polyimide P84® supports

P84® (HP Polymer GmbH) with crosslinking is chosen as support since it is going to be used for both water and organic solvent treatment. This support were prepared following a method adapted from the literature [27]. Briefly, a solution of P84® at 24 wt% was prepared in dimethylsulfoxide (DMSO, 99.2%, PanReac AppliChem®) by stirring overnight at room temperature. The solution was cast on a polypropylene non-woven backing material with an automatic film applicator (Elcometer 4340) at 0.04 m·s^{-1} and selecting a thickness of 250 μm. The film was promptly immersed in a bath of deionized water for the phase inversion for 10 min. Then it was transferred to a fresh water bath and left for 1 h. The film was immersed in two consecutive baths of 2-propanol (IPA, HPLC grade, ≥99.9%, PanReac AppliChem®) for 1 h each to remove the residual DMSO and water. P84® supports were posteriorly cross-linked by immersion in a 120 g·L^{-1} hexanediamine (HDA, 98%, Sigma-Aldrich) solution in IPA for 16 h under stirring. Then the supports were washed with fresh IPA four times for 1 h each to remove excess HDA. P84® supports were immersed in a 2/3 (v/v) IPA/polyethylene glycol (PEG, synthesis grade, PanReac AppliChem®) solution overnight to prevent from pore collapse. Finally, the supports were wiped with tissue paper.

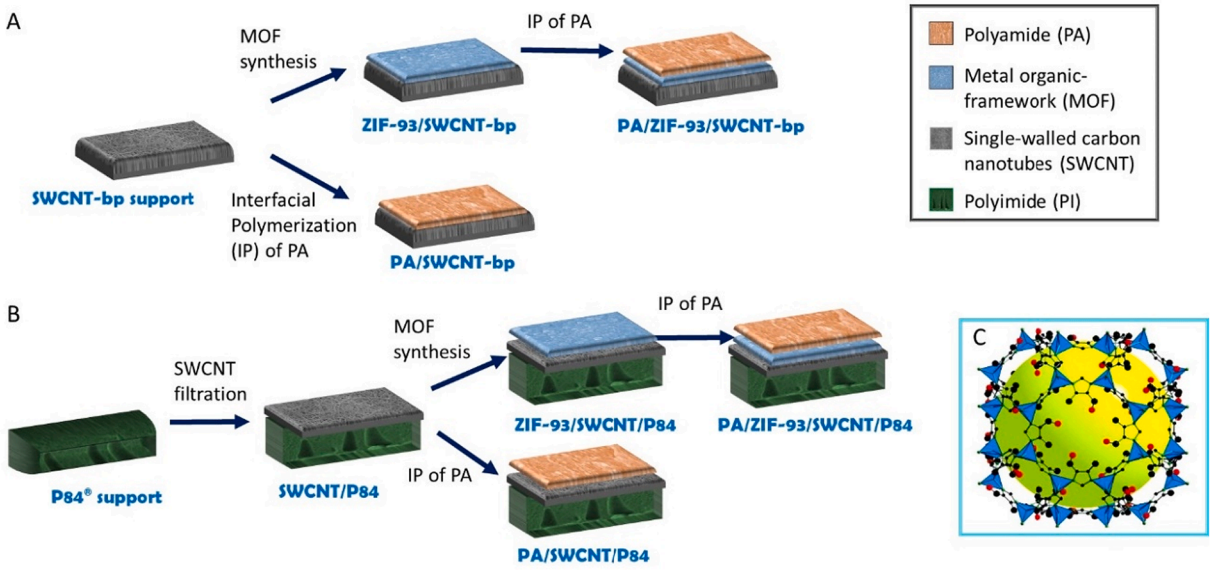

Fig. 1. A) Scheme of membranes used in our previous work [24]. B) Scheme of membranes used in this work. C) ZIF-93 representation corresponding to the RHO type structure, made with ZIF-93 CIF file [25] using Diamond 3.2 [26]. ZnN_4 tetrahedral clusters are shown in blue, C atoms in black, O atoms in red and the yellow sphere is the cavity. H atoms have been omitted for clarity.

2.2. Preparation of SWCNT/P84 membrane

The preparation of the single-walled carbon nanotubes (SWCNT, diameter 1.2–2 nm, 5 μm in length, ≥93% carbon content, Sigma-Aldrich) layer was performed by vacuum filtration on the previously prepared P84® support. The method was basically the one previously used to prepare SWCNT buckypapers [24] with the exception that lower concentrations and amounts of the carbon nanotubes were used here. The SWCNT loading was varied until finding the minimum amount of SWCNT that, after carrying out the IP of the PA layer, gave satisfactory results in nanofiltration. In order to have a better control of the concentrations, 100 mg of SWCNT was dispersed in 100 mL of a water solution containing 1 wt% of Triton X-100 (Sigma-Aldrich) surfactant using an ultrasonic probe sonicator (GEX750 ultrasonic processor, 750 W, 20 kHz) for 1 h. Then a 500 μL aliquot of the SWCNT dispersion was diluted with 50 mL of deionized water and dispersed with the probe sonicator for 10 min. This dispersion was then vacuum filtered through the P84® support placed in a glass filtration holder with a cellulose membrane filter (pore size 7 to 9 μm, diameter of 90 mm and 290 μm thickness, Prat Dumas). After filtration, the membrane was washed with a mixture of solvents IPA and acetone (99%, PanReac AppliChem®) [28].

2.3. Preparation of ZIF-93/SWCNT/P84 membrane

The synthesis of ZIF-93 on the SWCNT/P84 membrane was carried out following our optimized reported method on SWCNT-bp support at room temperature. [24]. The SWCNT/P84 membrane was placed vertically between a metallic ring and a metallic disc, avoiding the synthesis of the MOF on the side where the carbon nanotubes were not deposited. The following consecutive steps were performed twice: 1) immersion in 10 mM zinc nitrate ($Zn(NO_3)_2{\cdot}6H_2O$, reagent grade, Scharlau) methanolic solution for 30 min; 2) rinsed in pure methanol (MeOH, HPLC grade, ≥99.9%, PanReac AppliChem®) for 1 min; 3) immersion in a 20 mM 4-methyl-5-imidazolecarboxaldehyde (4-m-5-ica, 99%, Acros Organics) ligand solution in MeOH for 24 h; 4) rinsed again in pure MeOH for 1 min. After completing the four steps twice, the membrane with the MOF layer was washed with methanol for 10 min and dried overnight at room temperature. To discern the effect of the SWCNT layer, a ZIF-93/P84 membrane was prepared using the same steps indicated above for the synthesis of ZIF-93, but in this case directly on the P84® support.

2.4. Preparation of PA/SWCNT/P84 and PA/ZIF-93/SWCNT/P84 membranes

The PA layers were prepared by inverse interfacial polymerization (iIP) following a previously reported method [24] with the SWCNT/P84 and the ZIF-93/SWCNT/P84 membranes. In that previous work, membranes prepared by iIP showed higher nanofiltration yields than membranes prepared by conventional IP. With the membrane placed in a glass holder, the following steps were performed consecutively at room temperature: 1) soaked in fresh n-hexane (extra pure, Scharlau) for 10 min; 2) addition of 20 mL of a 0.1 wt% 1,3,5-benzenetricabonyl trichloride (TMC 98%, Sigma-Aldrich) solution in hexane for 5 min; 3) removal of organic solution with tissue paper; 4) IP with 20 mL of a 2 wt % m-phenylenediamine (MPD, 99%, Sigma-Aldrich) solution in water for 2 min; 5) to stop the reaction, removal of the aqueous solution and washing successively with fresh n-hexane and deionized water. After all the previous steps, the membrane with the PA layer was stored in deionized water in a refrigerator to be tested within the next 48 h.

2.5. Characterization

Various characterization techniques were used such as water contact angle (WCA), atomic force microscopy (AFM), X-ray diffraction (XRD), attenuated total reflection - Fourier transform infrared spectroscopy (ATR-FTIR) and scanning electron microscopy (SEM) coupled with focus ion beam (FIB). The equipment used to perform these characterization of the membrane samples and some of their most relevant features can be found in Table S1.

2.6. Nanofiltration experiments

Nanofiltration experiments were carried out in the two different set-ups described previously [24]: a stirred dead-end membrane filtration cell (Sterlitech HP4750) filled with 250 mL of solution and a cross-flow nanofiltration unit with a feed flow of 1 $L{\cdot}min^{-1}$. In both set-ups, the experiments were carried out at room temperature and 10 bar feed pressure using aqueous or methanolic feeds of 20 $mg{\cdot}L^{-1}$ of rose Bengal (RB, 95% dye content, Sigma Aldrich), sunset yellow (SY, 90% dye content, Sigma Aldrich) or acridine orange (AO, 55% dye content, Acros Organics). These dyes would simulate the wastewater produced in various industries (textile, rubber, packaging, leather tanning, pharmaceutical products, paper and plastic, among others)[29].

In the dead-end NF set-up, the measurements were first carried out with methanolic solutions, starting with the RB dye, then with SY dye and finally with AO dye, then the same procedure was repeated with aqueous solutions of the dyes. The measurements were at steady state, usually reached after 3 h under stream. If the module decreased its solution volume below 20% it was refilled with fresh solution. In cross-flow nanofiltration, only the RB dye was measured in aqueous solution with a typical duration of 6 h. However, one selected membrane was tested for up to ten days where during the night the experiment was stopped but the membrane was kept in contact with the RB solution.

The permeance ($L{\cdot}m^{-2}{\cdot}h^{-1}{\cdot}bar^{-1}$) and the rejection (%) values were calculated by Eqs. (1) and (2), respectively:

$$Permeance = \frac{V}{\Delta P{\cdot}A{\cdot}t} \tag{1}$$

$$Rejection(\%) = \left(1 - \frac{C_{permeate}}{C_{residue}}\right) \times 100 \tag{2}$$

where V (L) is the volume collected at time t (h), A (m^2) is the area of the NF membrane, ΔP (bar) is the pressure difference between the retentate and permeate sides; and $C_{permeate}/C_{residue}$ is the ratio between the permeate and residue concentrations.

The concentrations in water were measured by an UV spectrometer (JASCO V-670 spectrophotometer) at wavelengths of 549, 480 and 490 nm for RB, SY and AO, respectively. In the case of the methanolic solutions, methanol was evaporated and replaced by deionized water.

In addition to the NF experiments with dyes, dead-end NF was tested with 1.0 $g{\cdot}L^{-1}$ Na_2SO_4 (≥99%, Sigma-Aldrich) or NaCl (≥99%, Sigma-Aldrich) aqueous solutions. SevenMulti™ pH/conductivity meter (Mettler Toledo) was used to measure the concentrations. The concentration of dyes and salts were chosen so that the results are comparable to our previous work [24].

Finally, to study the stability in chlorine, the membranes were immersed in 1000 ppm sodium hypochlorite solution (Merck, 6–14% active chlorine) for 1 h and subsequently thoroughly washed with water.

3. Results and discussion

3.1. Characterization of the membranes structure

As shown in Fig. 1B, two different membrane structures were prepared in this work, using in both cases the polyimide P84® support. In the first case, single walled carbon nanotubes (SWCNT) were used as an interlayer between the P84® and the polyamide (PA) selective layer (PA/SWCNT/P84 membrane). Whilst in the other type, a ZIF-93 continuous layer was grown on top of the SWCNT layer before the

synthesis of the PA (PA/ZIF-93/SWCNT/P84 membrane).

During the filtration process of SWCNT, ropes (bundles) of 30–50 nm were assembled by van der Waals forces to form a uniform porous and entangled network (see Fig. 2A which corresponds to the SWCNT/P84 membrane), in agreement with the preparation of buckypaper supports [30,31]. The amount of SWCNTs applied is estimated in 0.08 $g{\cdot}m^{-2}$ in contrast with the 15.72 $g{\cdot}m^{-2}$ used in our previous work [24], which is among the lowest values used by other researchers (0.03–0.36 $g{\cdot}m^{-2}$) [19,21]. Fig. 2C shows a cross section of the ZIF-93/SWCNT/P84 membrane where the triple layer structure can be observed in the absence of the top PA film. The thickness of the ZIF-93 layer is about 50 nm. Moreover, the SWCNT exhibit a preferential vertical alignment probably provoked by the shear force and mechanical stretch applied during the preparation for the SEM characterization giving rise to some expansion of the SWCNT structure. This would indicate a good interaction of the carbon nanotubes both with the polymeric support and the MOF layer, which undoubtedly confers stability to the prepared multilayer structure. In fact, shear and mechanical force have been used to favour the horizontal alignment of carbon nanotubes on a polymer support [32]. An example dealing with vertical alignment with similarities to the observed here is the preparation of a sandwich of SWCNT layer between two polymer layers, that creates a vertical alignment when separated by peeling [33]. Fig. 2B shows the surface of the ZIF-93 layer, which is formed by well intergrown crystals, continuous and without apparent defects, of a size of approximately 80–100 nm. This continuous layer was not obtained in the case of the ZIF-93 synthesis over the bare P84® support (Fig. S1) which is in concordance with previous work on flat P84® support [34].

SEM images of the surface of the PA/SWCNT/P84 and PA/ZIF-93/SWCNT/P84 membranes can be observed in Fig. 3A and C, both showing typical rough surface the so-called ridge and valley structures [35], as well as the presence of nodular forms that seem to predominate more in the sample with the ZIF layer. If Fig. 3C and Fig. S2, both, with the ZIF-93 layer is observed in more detail, many of the commented nodules are annular, placed in various positions with respect to the membrane surface, ranging from parallel to orthogonal to the support surface. These annular nodules will be discussed later. To observe the thickness of the membranes, the FIB technique was used to obtain cross section images (Fig. 3B, D) of both PA/SWCNT/P84 and PA/ZIF-93/SWCNT/P84 membranes. The images confirm in both cases thicknesses of around 400 nm for the SWCNT coating (similar to or below those found in previous works where carbon nanotubes were applied as a gutter layer element) [12,36]. In these images, no vertical alignment of the carbon nanotubes can be seen, confirming that the aforementioned alignment probably occurred during the preparation of the sample for its observation by SEM. In addition, a certain porosity of the SWCNT layer is observed, which may be beneficial for its flow through. SEM images of PA/SWCNT/P84 membrane (Fig. 3B) allow to estimate a 40–60 nm thickness for the PA layer. In the PA/ZIF-93/SWCNT/P84 membrane, the PA layer is difficult to distinguish from that of the ZIF. The PA/ZIF-93 assembly has a thickness of 60–80 nm. This suggests the penetration of the polyamide in the layer of ZIF-93 to give a well interpenetrated area suggesting for the PA film a lower thickness value of ca. 10–30 nm in contrast to the layer directly synthesized on the SWCNT. This lower thickness would again result in a greater flow as well as the absence of defects would favour rejections. Besides, the aldehyde group of this MOF can help establish a stronger chemical interaction with the polyamide, through the formation of hydrogen bondings, than the expected on the bare carbon nanotube surface.

XRD (Fig. 4A) studies confirm the presence of the highly crystalline ZIF-93 on ZIF-93/SWCNT/P84 membrane with the presence of the most intense peak of ZIF-93 at 2 theta = 7.46°, while the absence of the rest of the peaks is due to the small thickness of the ZIF layer (≈50 nm). The presence of relatively intense peaks (14°, 17°, 18.6°, 21.7° and 24°) correspond to the partially crystalline polypropylene non-woven support [37] on which the P84® film was prepared by phase inversion as described in the experimental section. The SWCNT layer could not be detected by this technique in the membranes due to its low crystallinity [38]. Finally, once the polyamide was placed on top of the complex membrane, ZIF-93 could not be detected by XRD (not shown) due to the shielding generated.

ATR-FTIR spectra (Fig. 4B) further confirms the growth of the ZIF layer due to the appearance of the characteristic bands at 1630 and 1659 cm^{-1} related to the aldehyde group CHO [40] and the band 1493 cm^{-1} related to the C = C bond [14]. These bands are clearly visible on samples ZIF-93/SWCNT/P84 and PA/ZIF-93/SWCNT/P84. Other bands related to ZIF-93 (between 1600 cm^{-1} and 800 cm^{-1} [41]) are visible only on sample ZIF-93/SWCNT/P84. The FTIR absorbance bands that may be related to PA overlap with those of the P84® support, so their clear detection was not possible. In the same way, no characteristic bands of carbon nanotubes were detected, which are probably masked by the support.

Water contact angle measurements (Fig. 5) show an increment in the hydrophobicity when the carbon nanotubes are deposited on top of the polyimide support from WCA = 25.8° to WCA = 80.1°, which is slightly lower angle than the observed for the carbon nanotube buckypapers used in our previous work (WCA = 83.0°) [24]. It must be taken into account that in that work the SWCNT buckypapers were self-supported with a thickness of 15 μm while here they are supported on P84® and with a thickness of 400 nm, even so both contact angles are very similar. However, the hydrophilicity increases when the PA layer was synthesized on top of the SWCNT (WCA = 69.5° for PA/SWCNT/P84 membrane) and more when ZIF-93 was used as intermediate layer (WCA = 56.0° for PA/ZIF-93/SWCNT/P84 membrane). The latter is undoubtedly due to the hydrophilic character of ZIF-93, the membrane with ZIF-93 and without PA being the one that shows the lowest value of WCA (43.0°).

The AFM images of Fig. 6 and Fig. S3, where larger sections of all the membranes are shown, corroborate the appearance of the surfaces as well as the sizes observed by SEM. Bundles of SWCNTs with diameters of

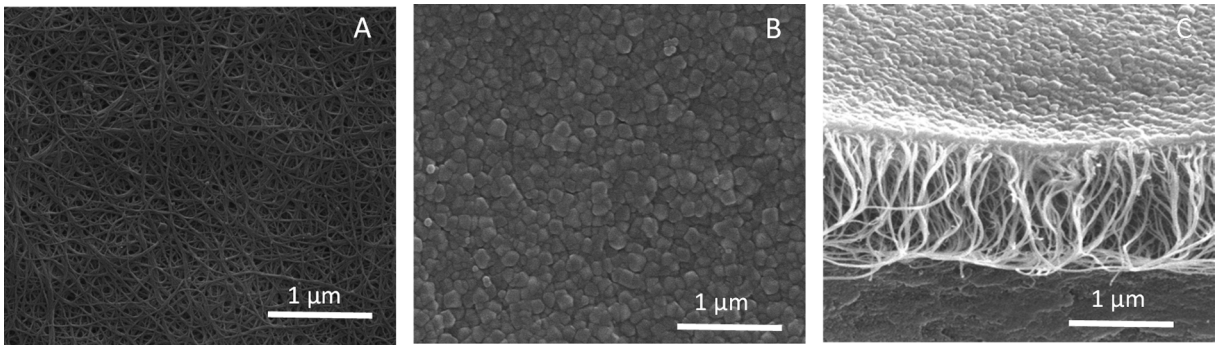

Fig. 2. SEM images of: A) Surface of the SWCNT/P84. B) Surface of ZIF-93/SWCNT/P84. C) Cross section of ZIF-93/SWCNT/P84.

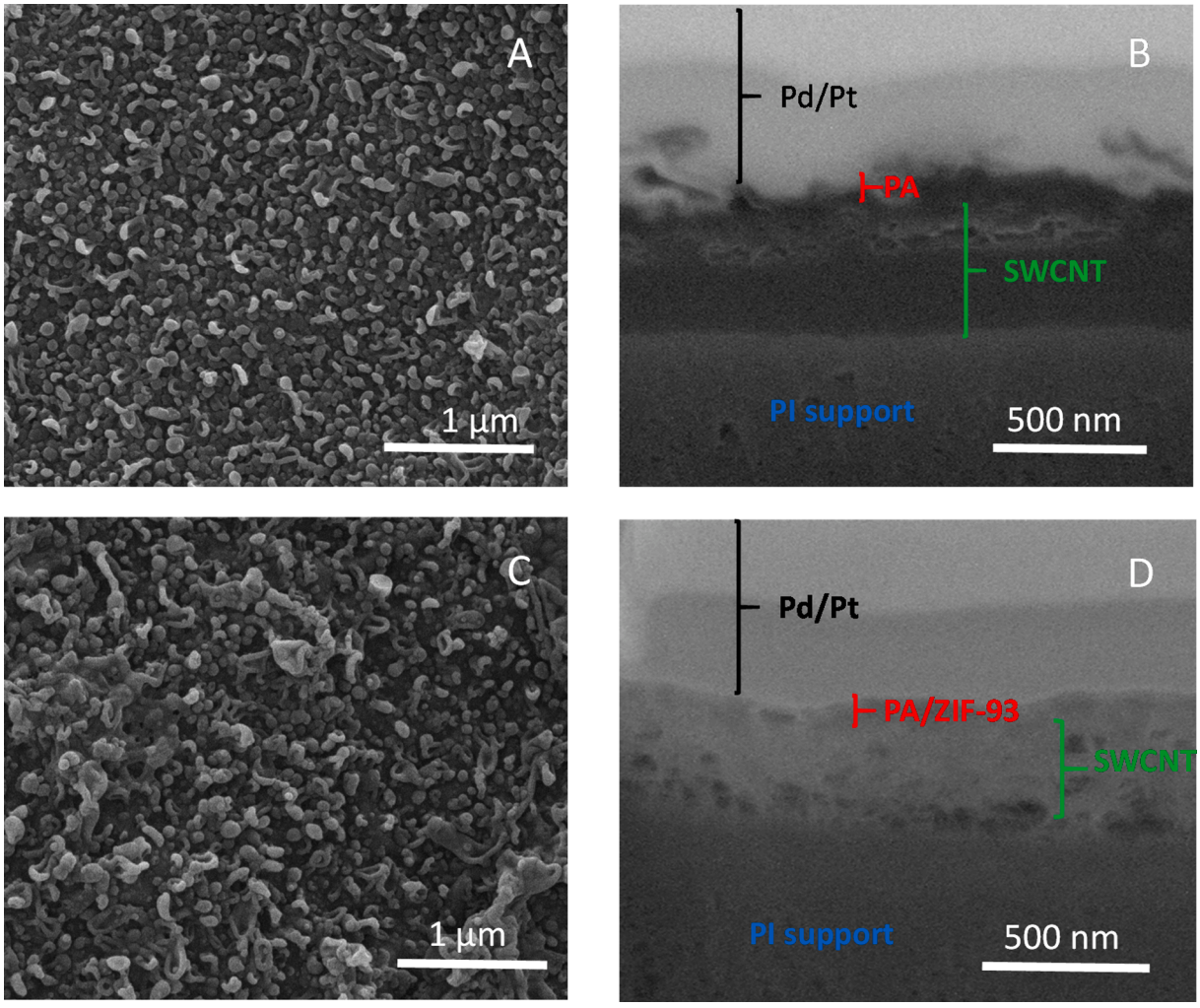

Fig. 3. SEM images: A) Surface of the PA/SWCNT/P84. C) Surface of PA/ZIF-93/SWCNT/P84. FIB-SEM images: B) PA/SWCNT/P84. D) PA/ZIF-93/SWCNT/P84.

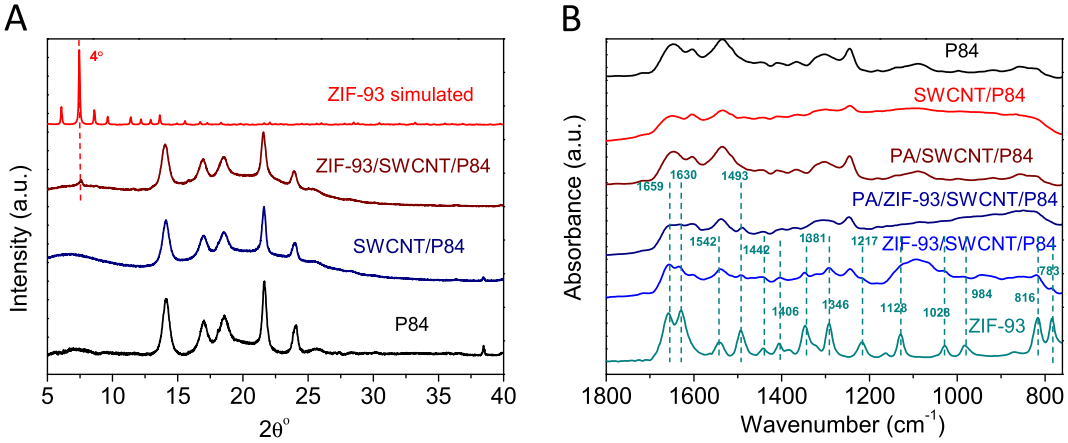

Fig. 4. A) XRD patterns. B) ATR-FTIR spectra. The simulated ZIF-93 XRD pattern was obtained using the corresponding CIF file [39].

30–50 nm and intergrown MOF crystals of size 80–100 nm were observed by AFM on the SWCNT/P84 (Fig. 6A) and on the ZIF-93/SWCNT/P84 (Fig. 6C) membranes, respectively. The surfaces of the membranes with the PA layer (Fig. 6B,D) show the presence of nodules that in the PA layer synthesized on MOF are more abundant and mostly annular with 80–100 nm in size. The formation of the morphology of the polyamide layer has been explained by various hypotheses, sometimes contradictories, ranging from local heating, "volcano-like" model, diffusion rate of the reagents and generation of nanobubbles[42,43]. Therefore, the morphology of the PA layer can be influenced by the order of the phases in the IP [44], the properties (porosity, pore size and hydrophilicity/hydrophobicity) of the sublayer[42] and the concentrations of the monomers have been reported [45]. Specifically, it has been argued that at very low concentrations of TMC annular nodules can be

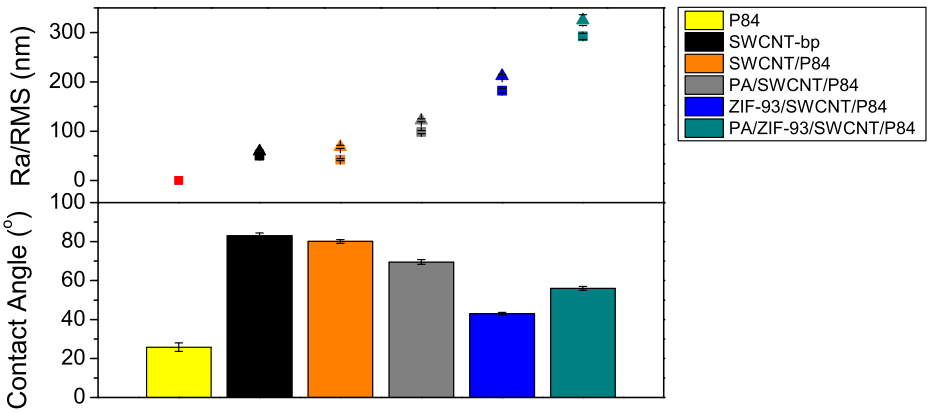

Fig. 5. Water contact angle, and Ra (average roughness, squares) and RMS (root mean square roughness, triangles) measured by AFM. Values can be found in Table S2.

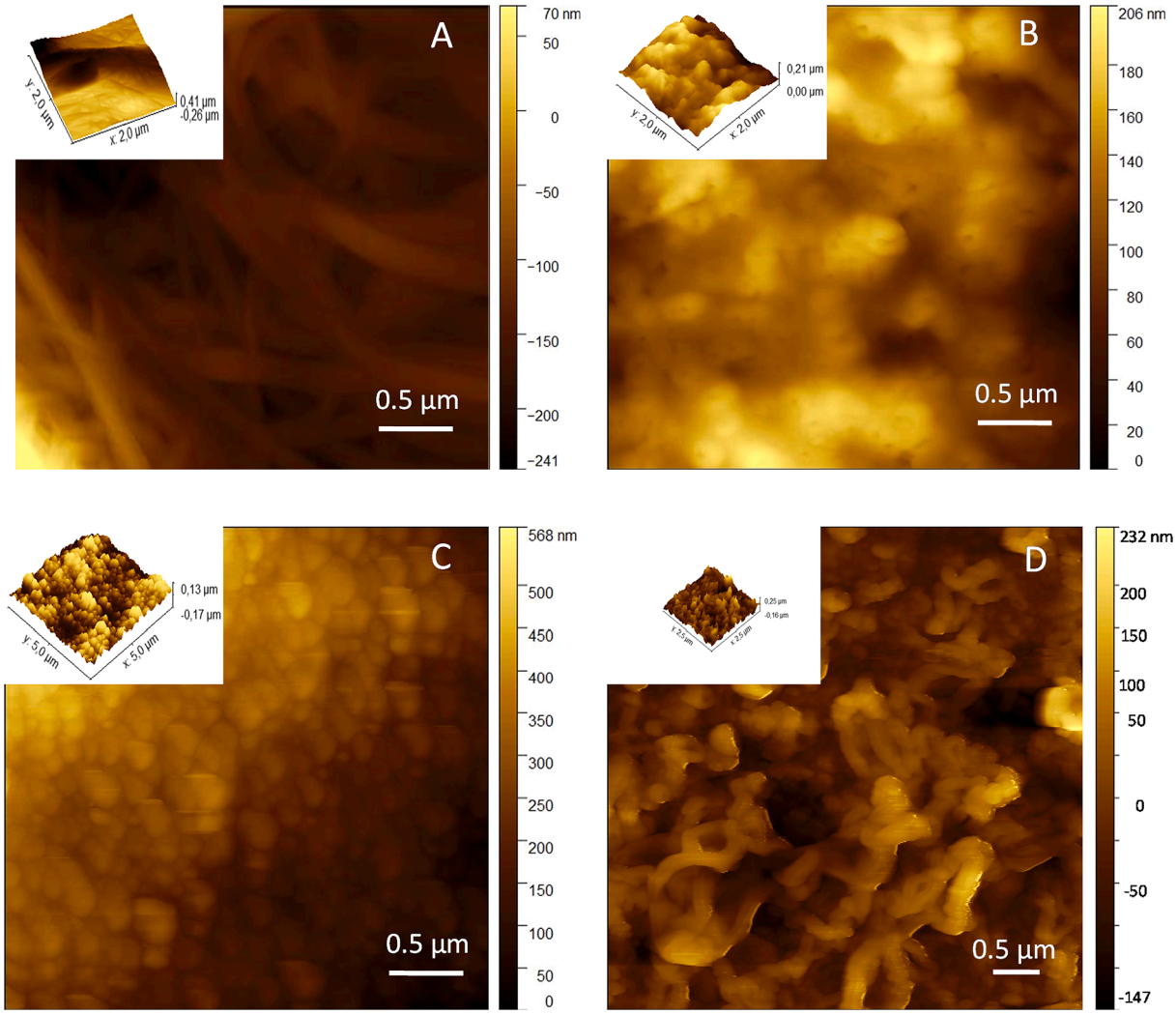

Fig. 6. AFM images: A) SWCNT/P84. B) PA/SWCNT/P84. C) ZIF-93/SWCNT/P84. D) PA/ZIF-93/SWCNT/P84.

formed [46]. This can explain the morphology of our PA skin layers, since the complex support was first impregnated with the organic phase with TMC in low concentration (0.2 wt%) and then impregnated with the aqueous phase with MPD in a higher concentration (2 wt%). In addition, the local concentration of TMC would be lower with the hydrophilic ZIF-93, which would retain less organic phase and therefore favouring the formation of annular nodules. Finally, the low monomers concentrations would decrease the IP kinetic giving rise to thinner layers, implying higher permeances [47].

Average roughness (Ra) and root mean square roughness (RMS) values were calculated from AFM images (Fig. 6). The results (Fig. 5) show an increase in the roughness of the membrane surface in the

following order: SWCNT/P84 ≈SWCNT-bp < PA/SWCNT/P84 < ZIF-93/SWCNT/P84 < PA/ZIF-93/SWCNT/P84. The roughness of the SWCNT layer on the polyimide support (SWCNT/P84) has a value very similar to that of the self-supported SWCNTs (SWCNT-bp). This agrees with the previous characterizations showing that there are no relevant physicochemical differences between both SWCNT surfaces. The polyamide layer and, to a greater extent, the ZIF layer increase the roughness with respect to the support, this effect being greater when the two layers are present, in agreement with previous works [13,24]. An increment in the surface roughness is associated with a higher effective area, enhancing the permeance in concordance with the nanofiltration results shown below. Also, according to the Wenzel equation [48], for the same hydrophilic material and increase of roughness generates a decrease of WCA.

3.2. Nanofiltration performance of PA/SWCNT/P84 and PA/ZIF-93/SWCNT/P84 membranes

Both the P84® support and SWCNT/P84 membrane have permeances higher than 1000 $L{\cdot}m^{-2}{\cdot}h^{-1}{\cdot}bar^{-1}$ with no appreciable rejection to any of the solutes studied. For the PA/SWCNT/P84 and PA/ZIF-93/SWCNT/P84 membranes, Fig. 7 shows permeance (Fig. 7A) and rejection (Fig. 7B) values obtained in a dead-end nanofiltration module filtering solutions of three different dyes (RB (1017 Da), SY (452 Da) and AO (265 Da)) in water (nanofiltration, NF) and methanol (organic solvent nanofiltration, OSN). The PA/SWCNT/P84 membrane shows interesting permeances and rejections but the PA/ZIF-93/SWCNT/P84 outperforms it in all cases with maximum permeance values of 57.6 ± 5.2 $L{\cdot}m^{-2}{\cdot}h^{-1}{\cdot}bar^{-1}$ and 84.5 ± 5.9 $L{\cdot}m^{-2}{\cdot}h^{-1}{\cdot}bar^{-1}$ for water and methanol, respectively, and rejections of 99.9 ± 3.3% (RB), 99.7 ± 3.5% (SY) and 99.6 ± 3.8% (AO) for NF experiments, and 99.8 ± 4.1% (RB), 99.5 ± 3.8% (SY) and 98.8 ± 3.5% (AO) for OSN experiments. These results show that the membrane can reject molecules with a molecular size as small as 265 Da with high solvent permeances. Therefore, these membranes would basically cover the range that is usually established for the nanofiltration application. With the dyes measured, the "molecular weight cut-off" of the membranes can be around 265 Da; however, the interactions established by the dyes make advisable to take this value with caution. It should be noted that the results given in Fig. 7 correspond to the average of the measurements of at least three different membranes prepared in the same conditions. The values do not have a very high standard deviation, indicating a good reproducibility of both the membrane preparation procedures and separation measurements carried out.

The high permeances and rejections that occur with the PA/SWCNT/P84 membrane have already been explained in our previous work [24] and are due to the fact that the SWCNT layer is able to control the monomers concentration during the IP process, so that a thinner, dense and defect-free PA layer is obtained. The characterization discussed above delves into these explanations as supported by the microscopy images and also in agreement with other works in the literature where an intermediate carbon nanotubes layer between the asymmetric support and the PA layer improves the filtration processes [12,36,49–51].

The improvement in the nanofiltration that occurs with the ZIF-93 layer seems to be related to several factors. a) The enhanced hydrophilicity of the membrane measured by WCA. b) Its greater roughness estimated by AFM. c) The microporous structure of ZIF-93 favoring the transport of the small solvent molecules. d) The porosity of the SWCNT layer observed by SEM. e) The gutter layer effect of the SWCNTs allowing the control of the synthesis of the MOF and indirectly that of the PA layer giving rise a thinner layer but of good quality to increase not only the flow but also the rejection. Besides, the characterizations done and results achieved with this PA/MOF layers are in agreement with previous works [24,34]. In fact, it is worth mentioning from the comparisons done in Fig. 7, that the current results based on the use of the polyimide supports (PA/ZIF-93/SWCNT/P84 membranes) even improve our previous results achieved with a support based only on SWCNTs (PA/ZIF-93/SWCNT-bp membranes [24]), the former consuming a 0.5% of the expensive SWCTs applied to prepare the SWCNT-bp support of the same area. The slight improvements in the water and methanol permeances could be due to the rigidity of the polypropylene/polyimide support as compared to the flexibility of the SWCNT-bp (suggested by the expansion of the SWCNT structure shown in Fig. 2C), whose contribution to the transport resistance would increase more upon compression. In any event, it should be noted that the results of our previous work were clearly among the best results in the literature, therefore the membranes prepared here are at the same level.

Salt rejection experiments with Na_2SO_4 and NaCl solutions were also

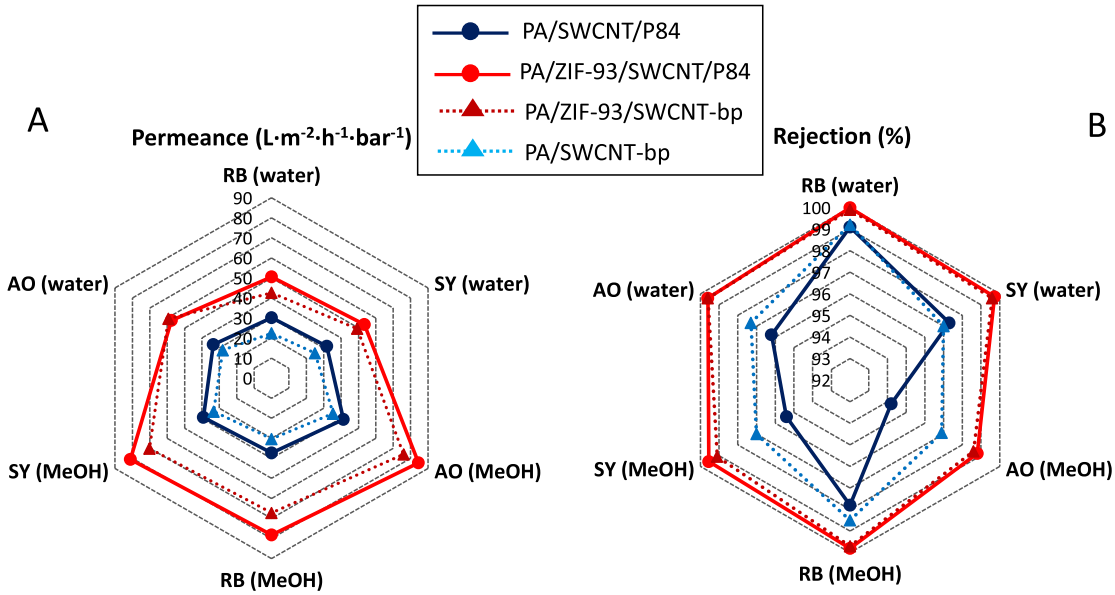

Fig. 7. Nanofiltration experiments on PA/SWCNT/P84 (blue) and PA/ZIF-93/SWCNT/P84 (red) membranes compared with the results of our previous work [24] (pointed lines) with PA/SWCNT (blue) and PA/ZIF-93/SWCNT (red) membranes: A) Permeances. B) Rejections. Values for both NF and OSN can be found in Tables S3 and S4.

performed in the dead-end nanofiltration module (Fig. 8) reaching rejections of 94.0 ± 3.9% and 17.9 ± 4.1% and permeances of 33.5 ± 3.1 $L{\cdot}m^{-2}{\cdot}h^{-1}{\cdot}bar^{-1}$ for the PA/SWCNT/P84 membrane and rejections of 94.8 ± 4.8% and 21.9 ± 3.6% with permeances of 55.7 ± 3.3 $L{\cdot}m^{-2}{\cdot}h^{-1}{\cdot}bar^{-1}$ for the PA/ZIF-93/SWCNT/P84. Very similar rejection results for both types of membranes, but with a clear water permeance increase in the membrane with the ZIF layer. These results are in concordance with the tendency observed in literature [52] related to the Donnan effect [53] leading to the better exclusion for high valence anions and lower rejections for monovalent anions, which is a typical behavior of a nanofiltration membrane.

Chlorine stability experiments were performed measuring the Na_2SO_4 rejection (Fig. 8) in the dead-end nanofiltration module for both types of membranes after being exposed to a NaOCl 1000 ppm solution for 1 h at room temperature [24]. The results show a slight decrease in rejection and a slight increase in permeation, which indicate that the stability of the membranes was not affected by the treatment, making them suitable for wastewater and desalination treatment applications were chlorine resistance is a major drawback for PA membranes [54]. Therefore, the presence of the ZIF-93 layer, that gives a better performance in nanofiltration, does not compromise the chlorine stability of the membrane.

Cross-flow experiments were performed with RB in water for 6 h (Fig. 9 and Table S6) until stabilization of the membrane at a permeance of 30 ± 2.9 $L{\cdot}m^{-2}{\cdot}h^{-1}{\cdot}bar^{-1}$ and rejection of 99.1 ± 2.5% for the PA/SWCNT/P84 membrane and 50.9 ± 3.3 $L{\cdot}m^{-2}{\cdot}h^{-1}{\cdot}bar^{-1}$ and 99.9 ± 1.9% for the PA/ZIF-93/SWCNT/P84. Almost identical results to those provided by the dead-end experiments confirming the reliability of the membranes. Additionally, for the PA/ZIF-93/SWCNT/P84 a long-term experiment was performed in the cross-flow nanofiltration module for a total duration of 10 days (Fig. 9). This experiment showed a great stability of the membrane over time with a minor drop (less than 2%) in permeance in the first 24 h of the experiment but maintaining it at 50 $L{\cdot}m^{-2}{\cdot}h^{-1}{\cdot}bar^{-1}$ for the rest of the experiment. The initial decrease in permeance could be related to a compression of the membrane at the beginning of the filtration when the membrane is exposed for the first time to the high operation pressure. It can be seen that the result is very similar to that of the 6 h experiments carried out with the other membranes, indicating once more the high reproducibility of the experimental methodology. The rejection was almost constant during the experiment duration (99.9%). Furthermore, the stability of the nanofiltration results seem to indicate that under working conditions the adsorption of the dye is not appreciable and the rejection mechanism is related to the size exclusion without ruling out the possibility of aggregation or charge of the dyes.

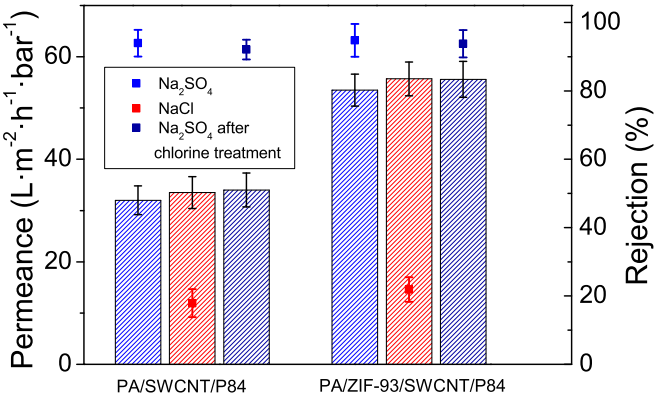

Fig. 8. Salt rejection nanofiltration experiments showing the permeance (bars) and rejection (square symbols) for both types of membranes for Na_2SO_4 (blue) and NaCl (red). Na_2SO_4 rejection experiments after chlorine treatment of the membranes are shown in dark blue. Values can be found in Table S5.

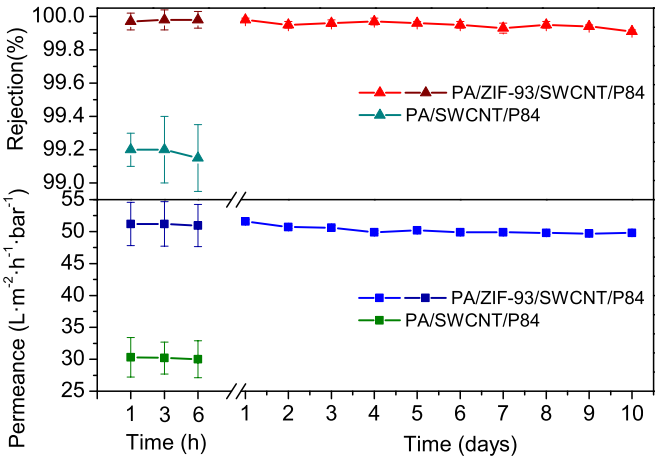

Fig. 9. Cross-flow experiments for PA/SWCNT/P84 and PA/ZIF-93/SWCNT/P84 for a duration of 6 h (error bars come from the testing of 3 different membranes). Long-term nanofiltration experiment for the PA/ZIF-93/SWCNT/P84 membrane with RB in water in the cross-flow module for an estimated time of 10 days (negligible error bars come from different measurements for the same membrane).

4. Conclusions

The synthesis of a PA film by interfacial polymerization on a SWCNT layer deposited by filtration on a polymeric support of polyimide P84® allows one to obtain a multi-layer membrane architecture, which can be further improved by the crystallization of ZIF-93 on top of the carbon nanotubes before the formation of the PA layer. As compared to our previous work, where the support for the ZIF-93 and PA was made only of SWCNTs, the polyimide reduces the SWCNT layer thickness to only 400 nm meaning in turn a 99.5% decrease of the use of SWCNTs to prepare the same membrane area. This would reduce tremendously the fabrication cost of the membrane due to the high price of CNTs.

The PA/ZIF-93/SWCNT/P84 membrane depicts the best results for both NF and OSN showing permeances of 57.6 ± 5.2 $L{\cdot}m^{-2}{\cdot}h^{-1}{\cdot}bar^{-1}$ and 84.5 ± 5.9 $L{\cdot}m^{-2}{\cdot}h^{-1}{\cdot}bar^{-1}$ for water and methanol, respectively, with rejections of 99.9 ± 3.3% (RB), 99.7 ± 3.5% (SY) and 99.6 ± 3.8% (AO) for water nanofiltration experiments, and 99.8 ± 4.1% (RB), 99.5 ± 3.8% (SY) and 98.8 ± 3.5% (AO) for methanol nanofiltration experiments. The improvement observed with the ZIF-93 layer seems to be related to the coupling of several factors which are: higher hydrophilicity of the membrane, higher surface roughness, the microporous structure of ZIF-93, the porosity of the carbon nanotubes layer and the control in the PA synthesis achieving a thinner layer thanks to the gutter layer effect that the SWCNTs exert on the MOF ZIF-93 synthesis and indirectly on the PA polymerization.

All these unique features yield also good separation performance in nanofiltration experiments dealing with desalination, achieving good rejections for divalent anions (94.8 ± 4.8%) and lower rejections for monovalent anions (21.9 ± 3.6%). Moreover, the membrane is stable once submitted to extreme conditions upon exposition to chlorine treatment, maintaining a high nanofiltration performance, which is a fundamental property in case of desalination applications.

The obtained results with the PA/ZIF-93/SWCNT/P84 complex membrane architecture, where the amount of the expensive component SWCNT is minimized, are among the best reported in the bibliography opening the door to highly efficient water treatment with organic pollutants and desalination, as well as to solvent recovery applications.

CRediT authorship contribution statement

Victor Berned-Samatán: Investigation, Methodology, Validation, Formal analysis, Visualization, Writing – original draft, Writing – review

& editing. **Marten Piantek:** Investigation, Validation, Formal analysis. **Joaquín Coronas:** Conceptualization, Methodology, Visualization, Supervision, Funding acquisition, Writing – original draft, Writing – review & editing. **Carlos Téllez:** Conceptualization, Methodology, Visualization, Supervision, Funding acquisition, Writing – original draft, Writing – review & editing.

Declaration of Competing Interest

The authors declare that they have no known competing financial interests or personal relationships that could have appeared to influence the work reported in this paper.

Data availability

Data will be made available on request.

Acknowledgements

Grant PID2019-104009RB-I00 funded by MCIN/AEI/10.13039/501100011033 is gratefully acknowledged (Agencia Estatal de Investigación (AEI) and Ministerio de Ciencia e Innovación (MCIN), Spain). Financial support from the Aragón Government is also gratefully acknowledged (T43-20R). V. B.-S. thanks the Grant BES-2017-080209 funded by MCIN/AEI/ 10.13039/501100011033 and by "ESF Investing in your future". The authors would like to acknowledge the use of the Servicio General de Apoyo a la Investigación-SAI and the use of instrumentation as well as the technical advice provided by the National Facility ELECMI ICTS, node "Laboratorio de Microscopias Avanzadas" at the University of Zaragoza.

Appendix A. Supplementary material

Supplementary data to this article can be found online at https://doi.org/10.1016/j.seppur.2022.122915.

References

[1] X. He, M.-B. Hägg, Membranes for environmentally friendly energy processes, Membranes (Basel). 2 (2012) 706–726, https://doi.org/10.3390/membranes2040706.
[2] A.W. Mohammad, Y.H. Teow, W.L. Ang, Y.T. Chung, D.L. Oatley-Radcliffe, N. Hilal, Nanofiltration membranes review: Recent advances and future prospects, Desalination. 356 (2015) 226–254, https://doi.org/10.1016/j.desal.2014.10.043.
[3] M. Paul, S.D. Jons, Chemistry and fabrication of polymeric nanofiltration membranes: A review, Polymer (Guildf). 103 (2016) 417–456, https://doi.org/10.1016/j.polymer.2016.07.085.
[4] P. Marchetti, M.F. Jimenez Solomon, G. Szekely, A.G. Livingston, Molecular Separation with Organic Solvent Nanofiltration: A Critical Review, Chem. Rev. 114 (2014) 10735–10806, https://doi.org/10.1021/cr500006j.
[5] V.V. Bhaskar, N.J. Kaleekkal, Next-generation thin-film composite nanofiltration membranes for water remediation: a review, Emergent Mater. (2021), https://doi.org/10.1007/s42247-021-00273-8.
[6] M.A. Abdel-Fatah, Nanofiltration systems and applications in wastewater treatment: Review article, Ain Shams Eng. J. 9 (2018) 3077–3092, https://doi.org/10.1016/j.asej.2018.08.001.
[7] B. Van der Bruggen, M. Mänttäri, M. Nyström, Drawbacks of applying nanofiltration and how to avoid them: A review, Sep. Purif. Technol. 63 (2008) 251–263, https://doi.org/10.1016/j.seppur.2008.05.010.
[8] C.Z. Liang, T.-S. Chung, J.-Y. Lai, A review of polymeric composite membranes for gas separation and energy production, Prog. Polym. Sci. 97 (2019), 101141, https://doi.org/10.1016/j.progpolymsci.2019.06.001.
[9] W.J. Lau, A.F. Ismail, N. Misdan, M.A. Kassim, A recent progress in thin film composite membrane: A review, Desalination. 287 (2012) 190–199, https://doi.org/10.1016/j.desal.2011.04.004.
[10] G.-R. Xu, J.-M. Xu, H.-J. Feng, H.-L. Zhao, S.-B. Wu, Tailoring structures and performance of polyamide thin film composite (PA-TFC) desalination membranes via sublayers adjustment-a review, Desalination. 417 (2017) 19–35, https://doi.org/10.1016/j.desal.2017.05.011.
[11] L. Paseta, C. Echaide-Górriz, C. Téllez, J. Coronas, Vapor phase interfacial polymerization: a method to synthesize thin film composite membranes without using organic solvents, Green Chem. 23 (2021) 2449–2456, https://doi.org/10.1039/d1gc00236h.
[12] L. Long, C. Wu, Z. Yang, C.Y. Tang, Carbon Nanotube Interlayer Enhances Water Permeance and Antifouling Performance of Nanofiltration Membranes: Mechanisms and Experimental Evidence, Environ. Sci. Technol. 56 (2022) 2656–2664, https://doi.org/10.1021/acs.est.1c07332.
[13] M. Navarro, J. Benito, L. Paseta, I. Gascón, J. Coronas, C. Téllez, Thin-Film Nanocomposite Membrane with the Minimum Amount of MOF by the Langmuir-Schaefer Technique for Nanofiltration, ACS Appl. Mater. Interfaces. 10 (2018) 1278–1287, https://doi.org/10.1021/acsami.7b17477.
[14] C. Echaide-Górriz, J.A. Zapata, M. Etxeberría-Benavides, C. Téllez, J. Coronas, Polyamide/MOF bilayered thin film composite hollow fiber membranes with tuned MOF thickness for water nanofiltration, Sep. Purif. Technol. 236 (2020), 116265, https://doi.org/10.1016/j.seppur.2019.116265.
[15] B. Zhao, Z. Guo, H. Wang, L. Wang, Y. Qian, X. Long, C. Ma, Z. Zhang, J. Li, H. Zhang, Enhanced water permeance of a polyamide thin-film composite nanofiltration membrane with a metal-organic framework interlayer, J. Membr. Sci. 625 (2021), 119154, https://doi.org/10.1016/j.memsci.2021.119154.
[16] Y. Wen, X. Zhang, X. Li, Z. Wang, C.Y. Tang, Metal-Organic Framework Nanosheets for Thin-Film Composite Membranes with Enhanced Permeability and Selectivity, ACS Appl. Nano Mater. 3 (2020) 9238–9248, https://doi.org/10.1021/acsanm.0c01860.
[17] Z. Zha, P. He, S. Zhao, R. Guo, Z. Wang, J. Wang, Interlayer-modulated polyamide composite membrane for organic solvent nanofiltration, J. Membr. Sci. 647 (2022), 120306, https://doi.org/10.1016/j.memsci.2022.120306.
[18] C. Yang, S. Li, X. Lv, H. Li, L. Han, B. Su, Effectively regulating interfacial polymerization process via in-situ constructed 2D COFs interlayer for fabricating organic solvent nanofiltration membranes, J. Membr. Sci. 637 (2021), 119618, https://doi.org/10.1016/j.memsci.2021.119618.
[19] M.-B.-B. Wu, Y. Lv, H.-C.-C. Yang, L.-F.-F. Liu, X. Zhang, Z.-K.-K. Xu, Thin film composite membranes combining carbon nanotube intermediate layer and microfiltration support for high nanofiltration performances, J. Membr. Sci. 515 (2016) 238–244, https://doi.org/10.1016/j.memsci.2016.05.056.
[20] S. Al Aani, A. Haroutounian, C.J. Wright, N. Hilal, Thin Film Nanocomposite (TFN) membranes modified with polydopamine coated metals/carbon-nanostructures for desalination applications, Desalination. 427 (2018) 60–74, https://doi.org/10.1016/j.desal.2017.10.011.
[21] M.J. Park, C. Wang, D.H. Seo, R.R. Gonzales, H. Matsuyama, H.K. Shon, Inkjet printed single walled carbon nanotube as an interlayer for high performance thin film composite nanofiltration membrane, J. Membr. Sci. 620 (2021), 118901, https://doi.org/10.1016/j.memsci.2020.118901.
[22] S. Gao, Y. Zhu, Y. Gong, Z. Wang, W. Fang, J. Jin, Ultrathin Polyamide Nanofiltration Membrane Fabricated on Brush-Painted Single-Walled Carbon Nanotube Network Support for Ion Sieving, ACS Nano. 13 (2019) 5278–5290, https://doi.org/10.1021/acsnano.8b09761.
[23] Y. Zhu, W. Xie, S. Gao, F. Zhang, W. Zhang, Z. Liu, J. Jin, Single-Walled Carbon Nanotube Film Supported Nanofiltration Membrane with a Nearly 10 nm Thick Polyamide Selective Layer for High-Flux and High-Rejection Desalination, Small. 12 (2016) 5034–5041, https://doi.org/10.1002/smll.201601253.
[24] V. Berned-Samatán, C. Rubio, A. Galán-González, E. Muñoz, A.M. Benito, W. K. Maser, J. Coronas, C. Téllez, Single-walled carbon nanotube buckypaper as support for highly permeable double layer polyamide/zeolitic imidazolate framework in nanofiltration processes, J. Membr. Sci. 652 (2022), 120490, https://doi.org/10.1016/j.memsci.2022.120490.
[25] W. Morris, B. Leung, H. Furukawa, O.K. Yaghi, N. He, H. Hayashi, Y. Houndonougbo, M. Asta, B.B. Laird, O.M. Yaghi, A combined experimental-computational investigation of carbon dioxide capture in a series of isoreticular zeolitic imidazolate frameworks, J. Am. Chem. Soc. 132 (2010) 11006–11008, https://doi.org/10.1021/ja104035j.
[26] Dr. H. Putz & Dr. K. Brandenburg, Diamond - Crystal and Molecular Structure Visualization, (n.d.).
[27] L. Paseta, J.M. Luque-Alled, M. Malankowska, M. Navarro, P. Gorgojo, J. Coronas, C. Téllez, Functionalized graphene-based polyamide thin film nanocomposite membranes for organic solvent nanofiltration, Sep. Purif. Technol. 247 (2020), 116995, https://doi.org/10.1016/j.seppur.2020.116995.
[28] J.A. Rojas, L.A. Ardila-Rodríguez, M.F. Diniz, M. Gonçalves, B. Ribeiro, M. C. Rezende, Optimization of Triton X-100 removal and ultrasound probe parameters in the preparation of multiwalled carbon nanotube buckypaper, Mater. Des. 166 (2019), 107612, https://doi.org/10.1016/j.matdes.2019.107612.
[29] X. Feng, D. Peng, J. Zhu, Y. Wang, Y. Zhang, Recent advances of loose nanofiltration membranes for dye/salt separation, Sep. Purif. Technol. 285 (2022), 120228, https://doi.org/10.1016/j.seppur.2021.120228.
[30] Z. Wang, Z. Liang, B. Wang, C. Zhang, L. Kramer, Processing and property investigation of single-walled carbon nanotube (SWNT) buckypaper/epoxy resin matrix nanocomposites, Compos. Part A Appl. Sci. Manuf. 35 (2004) 1225–1232, https://doi.org/10.1016/j.compositesa.2003.09.029.
[31] J.Y. Oh, S.J. Yang, J.Y. Park, T. Kim, K. Lee, Y.S. Kim, H.N. Han, C.R. Park, Easy Preparation of Self-Assembled High-Density Buckypaper with Enhanced Mechanical Properties, Nano Lett. 15 (2015) 190–197, https://doi.org/10.1021/nl5033588.
[32] P.S. Goh, A.F. Ismail, B.C. Ng, Directional alignment of carbon nanotubes in polymer matrices: Contemporary approaches and future advances, Compos. Part A Appl. Sci. Manuf. 56 (2014) 103–126, https://doi.org/10.1016/j.compositesa.2013.10.001.
[33] H. Zhao, Z. Zhou, H. Dong, L. Zhang, H. Chen, L. Hou, A facile method to align carbon nanotubes on polymeric membrane substrate, Sci. Rep. 3 (2013) 3480, https://doi.org/10.1038/srep03480.

[34] L. Paseta, D. Antorán, J. Coronas, C. Téllez, 110th Anniversary: Polyamide/Metal-Organic Framework Bilayered Thin Film Composite Membranes for the Removal of Pharmaceutical Compounds from Water, Ind. Eng. Chem. Res. 58 (2019) 4222–4230, https://doi.org/10.1021/acs.iecr.8b06017.

[35] F. Pacheco, R. Sougrat, M. Reinhard, J.O. Leckie, I. Pinnau, 3D visualization of the internal nanostructure of polyamide thin films in RO membranes, J. Membr. Sci. 501 (2016) 33–44, https://doi.org/10.1016/j.memsci.2015.10.061.

[36] S. Sun, L. Han, J. Hou, Y. Yang, J. Yue, G. Gu, C.Y. Chuah, J. Li, Z. Zhang, Single-walled carbon nanotube gutter layer supported ultrathin zwitterionic microporous polymer membrane for high-performance lithium-sulfur battery, J. Colloid Interface Sci. 628 (2022) 1012–1022, https://doi.org/10.1016/j.jcis.2022.08.025.

[37] P. Franciszczak, J. Wojnowski, K. Kalniņš, E. Piesowicz, The influence of matrix crystallinity on the mechanical performance of short-fibre composites – Based on homo-polypropylene and a random polypropylene copolymer reinforced with man-made cellulose and glass fibres, Compos. Part B Eng. 166 (2019) 516–526, https://doi.org/10.1016/j.compositesb.2019.02.046.

[38] V. Berned-Samatán, S. Jiménez, C. Rubio, C. Téllez, J. Coronas, Self-supported single-wall carbon nanotube buckypaper membranes applied to air and water fi ltration, J. Chem. Technol. Biotechnol. (2022) 1–6, https://doi.org/10.1002/jctb.7231.

[39] W. Morris, N. He, K.G. Ray, P. Klonowski, H. Furukawa, I.N. Daniels, Y. A. Houndonougbo, M. Asta, O.M. Yaghi, B.B. Laird, A combined experimental-computational study on the effect of topology on carbon dioxide adsorption in zeolitic imidazolate frameworks, J. Phys. Chem. C. 116 (2012) 24084–24090, https://doi.org/10.1021/jp307170a.

[40] J. Sánchez-Laínez, B. Zornoza, A.F. Orsi, M.M. Łozińska, D.M. Dawson, S. E. Ashbrook, S.M. Francis, P.A. Wright, V. Benoit, P.L. Llewellyn, C. Téllez, J. Coronas, Synthesis of ZIF-93/11 Hybrid Nanoparticles via Post-Synthetic Modification of ZIF-93 and Their Use for H2/CO2 Separation, Chem. - A Eur. J. 24 (2018) 11211–11219, https://doi.org/10.1002/chem.201802124.

[41] L. Sarango, J. Benito, I. Gascón, B. Zornoza, J. Coronas, Homogeneous thin coatings of zeolitic imidazolate frameworks prepared on quartz crystal sensors for CO2 adsorption, Microporous Mesoporous Mater. 272 (2018) 44–52, https://doi.org/10.1016/j.micromeso.2018.06.018.

[42] L.E. Peng, Z. Yang, L. Long, S. Zhou, H. Guo, C.Y. Tang, A critical review on porous substrates of TFC polyamide membranes: Mechanisms, membrane performances, and future perspectives, J. Membr. Sci. 641 (2022), 119871, https://doi.org/10.1016/j.memsci.2021.119871.

[43] H. An, J.W. Smith, B. Ji, S. Cotty, S. Zhou, L. Yao, F.C. Kalutantirige, W. Chen, Z. Ou, X. Su, J. Feng, Q. Chen, Mechanism and performance relevance of nanomorphogenesis in polyamide films revealed by quantitative 3D imaging and machine learning, Sci. Adv. 8 (2022) eabk1888, https://doi.org/10.1126/sciadv.abk1888.

[44] X. Song, B. Gan, Z. Yang, C.Y. Tang, C. Gao, Confined nanobubbles shape the surface roughness structures of thin film composite polyamide desalination membranes, J. Membr. Sci. 582 (2019) 342–349, https://doi.org/10.1016/j.memsci.2019.04.027.

[45] S. Habib, S.T. Weinman, A review on the synthesis of fully aromatic polyamide reverse osmosis membranes, Desalination. 502 (2021), 114939, https://doi.org/10.1016/j.desal.2021.114939.

[46] J. Xu, H. Yan, Y. Zhang, G. Pan, Y. Liu, The morphology of fully-aromatic polyamide separation layer and its relationship with separation performance of TFC membranes, J. Membr. Sci. 541 (2017) 174–188, https://doi.org/10.1016/j.memsci.2017.06.057.

[47] V. Freger, G.Z. Ramon, Polyamide desalination membranes: Formation, structure, and properties, Elsevier B.V. (2021), https://doi.org/10.1016/j.progpolymsci.2021.101451.

[48] B. Tylkowski, I. Tsibranska, Overview of main techniques used for membrane characterization, J. Chem. Technol. Metall. 50 (2014).

[49] L.-Y.-Y. Chen, M.-Y.-Y. Jiang, Q. Zou, S.-W.-W. Xiong, Z.-G.-G. Wang, L.-S.-S. Cui, H. Guo, T. Zhou, J.-G.-G. Gai, Highly permeable carbon nanotubes/polyamide layered membranes for molecular sieving, Chem. Eng. J. 425 (2021), 130684, https://doi.org/10.1016/j.cej.2021.130684.

[50] Y. Lu, Z. Wang, W. Fang, Y. Zhu, Y. Zhang, J. Jin, Polyamide Thin Films Grown on PD/SWCNT-Interlayered-PTFE Microfiltration Membranes for High-Permeance Organic Solvent Nanofiltration, Ind. Eng. Chem. Res. 59 (2020) 22533–22540, https://doi.org/10.1021/acs.iecr.0c04969.

[51] G. Gong, P. Wang, Z. Zhou, Y. Hu, New Insights into the Role of an Interlayer for the Fabrication of Highly Selective and Permeable Thin-Film Composite Nanofiltration Membrane, ACS Appl. Mater. Interfaces. 11 (2019) 7349–7356, https://doi.org/10.1021/acsami.8b18719.

[52] L.F. Liu, X. Huang, X. Zhang, K. Li, Y.L. Ji, C.Y. Yu, C.J. Gao, Modification of polyamide TFC nanofiltration membrane for improving separation and antifouling properties, RSC Adv. 8 (2018) 15102–15110, https://doi.org/10.1039/c8ra01374h.

[53] X. Wu, L. Yang, F. Meng, W. Shao, X. Liu, M. Li, ZIF-8-incorporated thin-film nanocomposite (TFN) nanofiltration membranes: Importance of particle deposition methods on structure and performance, J. Membr. Sci. 632 (2021), 119356, https://doi.org/10.1016/j.memsci.2021.119356.

[54] R. Verbeke, D.M. Davenport, T. Stassin, S. Eyley, M. Dickmann, A.J. Cruz, P. Dara, C.L. Ritt, C. Bogaerts, W. Egger, R. Ameloot, J. Meersschaut, W. Thielemans, G. Koeckelberghs, M. Elimelech, I.F.J. Vankelecom, Chlorine-Resistant Epoxide-Based Membranes for Sustainable Water Desalination, Environ. Sci. Technol. Lett. 8 (2021) 818–824, https://doi.org/10.1021/acs.estlett.1c00515.